Received: 26 January 2024 | Revised: 23 April 2024 | Accepted: 24 April 2024

DOI: 10.1002/alz.13900

Alzheimer's & Dementia®
THE JOURNAL OF THE ALZHEIMER'S ASSOCIATION

RESEARCH ARTICLE

Cognitive integrity in Non-Demented Individuals with Alzheimer's Neuropathology is associated with preservation and remodeling of dendritic spines

Jutatip Guptarak[1] | **Pietro Scaduto**[1] | **Batbayar Tumurbaatar**[1] | **Wen Ru Zhang**[1] | **Daniel Jupiter**[2] | **Giulio Taglialatela**[1] | **Anna Fracassi**[1]

[1]Department of Neurology, Mitchell Center for Neurodegenerative Disease, University of Texas Medical Branch at Galveston, Galveston, Texas, USA

[2]Department of Biostatistics and Data Science, University of Texas Medical Branch at Galveston, Galveston, Texas, USA

Correspondence
Anna Fracassi and Giulio Taglialatela, Department of Neurology, Mitchell Center for Neurodegenerative Disease, University of Texas Medical Branch at Galveston, 301 University Blvd, Galveston, TX, USA.
Email: anfracas@utmb.edu and gtaglial@utmb.edu

Funding information
NIH/NIA, Grant/Award Number: R21AG082230; Alzheimer's Association Research Fellowship, Grant/Award Number: AARF22973974; NIH/NIA, Grant/Award Numbers: R01AG069433, AG073133

Abstract

INTRODUCTION: Individuals referred to as Non-Demented with Alzheimer's Neuropathology (NDAN) exhibit cognitive resilience despite presenting Alzheimer's disease (AD) histopathological signs. Investigating the mechanisms behind this resilience may unveil crucial insights into AD resistance.

METHODS: DiI labeling technique was used to analyze dendritic spine morphology in control (CTRL), AD, and NDAN *post mortem* frontal cortex, particularly focusing on spine types near and far from amyloid beta (Aβ) plaques.

RESULTS: NDAN subjects displayed a higher spine density in regions distant from Aβ plaques versus AD patients. In distal areas from the plaques, NDAN individuals exhibited more immature spines, while AD patients had a prevalence of mature spines. Additionally, our examination of levels of Peptidyl-prolyl cis-trans isomerase NIMA-interacting 1 (Pin1), a protein associated with synaptic plasticity and AD, showed significantly lower expression in AD versus NDAN and CTRL.

DISCUSSION: These results suggest that NDAN individuals undergo synaptic remodeling, potentially facilitated by Pin1, serving as a compensatory mechanism to preserve cognitive function despite AD pathology.

KEYWORDS
Alzheimer's disease, amyloid beta, cognitive resilience, dendritic spines, neurodegeneration, Non-Demented with Alzheimer's Neuropathology, Pin1, synaptic plasticity

Highlights

- Spine density is reduced near Aβ plaques compared to the distal area in CTRL, AD, and NDAN dendrites.
- NDAN shows higher spine density than AD in areas far from Aβ plaques.
- Far from Aβ plaques, NDAN has a higher density of immature spines, AD a higher density of mature spines.
- AD individuals show significantly lower levels of Pin1 compared to NDAN and CTRL.

Jutatip Guptarak and Pietro Scaduto contributed equally to this study.

1 | BACKGROUND

Alzheimer's disease (AD), affecting nearly six million people in the United States, is a progressive neurodegenerative disorder characterized by memory and cognitive decline, disability, and ultimately death.[1] The disease's hallmark is the accumulation of extracellular amyloid beta (Aβ) plaques, primarily insoluble Aβ40-42 peptides, and intracellular neurofibrillary tangles of hyperphosphorylated tau peptide.[2,3] These accumulations are especially abundant in memory-essential brain regions like the entorhinal cortex, hippocampus, and cerebral cortex.[4–6] Recent studies suggest that Aβ plaques, combined with the accumulation of Aβ peptides and tau protein at synapses, cause neuronal structure changes such as axon and dendrite deformation, impacting synaptic integrity, plasticity, and dendritic spine maintenance, which are critical for neuronal connections.[7] These structural alterations disrupt synaptic integrity and plasticity, affecting dendritic spine maintenance and neuronal connectivity,[8–10] which precedes neuronal death and cognitive decline in AD.[11,12] However, a subset of individuals – classified as A+T+N–, where "A" refers to the value of an Aβ biomarker (amyloid positron emission tomography [PET] or cerebrospinal fluid [CSF] Aβ42), "T" the value of a tau biomarker (CSF phospho tau or tau PET), and "N" biomarkers of neurodegeneration or neuronal injury ([18F]-fluorodeoxyglucose–PET, structural magnetic resonance imaging, or CSF total tau)[13] – display AD-like neuropathological characteristics but without the associated cognitive decline. We here refer to these individuals as Non-Demented with Alzheimer's Neuropathology (NDAN).[14,15] Emerging research suggests that the structural plasticity of dendritic spines could play a crucial role in countering AD, allowing those individuals to evade dementia.[12,16] Those studies emphasize the importance of further investigating dendritic structures in these subjects to deepen our understanding of cognitive resilience mechanisms in AD. We previously reported that synapses of NDAN subjects displayed a unique proteomic profile and miRNA regulation,[17] and NDAN individuals have an increased number of neural stem cells in the hippocampus,[18] preserved antioxidant,[19] and autophagy response,[20] and their synapses are resistant to the detrimental binding of Aβ and tau oligomers.[21,22] Although NDAN and AD subjects exhibit comparable levels of pathological Aβ plaque deposition, NDAN individuals appear to be resistant to the well-documented effects of amyloid deposits on dendrites and axons, which typically lead to spine loss, dendritic atrophy, and axonal varicosities, culminating in widespread and permanent neural disruption.[11,23,24] This phenomenon could be attributed to a distinct microglial phenotype we found in NDAN subjects, with high phagocytic activity around Aβ plaques, that is associated with the removal of damaged synapses and preserved axonal structure.[25] The presence of this microglial subset points to a possible synaptic recycling mechanism, wherein damaged mature synapses are engulfed and subsequently replaced by newly formed synapses, potentially facilitating synaptic resilience and plasticity in NDAN brains.

In this study, we investigated potential synaptic variations among age-matched healthy subjects (CTRL), NDAN individuals, and AD subjects, whether near Aβ plaques or not, by examining dendritic spines.

RESEARCH IN CONTEXT

1. **Systematic review**: A literature review was conducted utilizing traditional sources, such as PubMed, to explore synaptic remodeling in AD and in individuals who are Non-Demented with Alzheimer's Neuropathology (NDAN). Few existing studies are focused on synaptic changes in AD, but they do not compare dendrite spines across control (CTRL), AD, and NDAN subjects in the context of amyloid beta (Aβ) pathology. Additionally, we selected Pin1 as a key factor that might be crucial in maintaining cognitive integrity in NDAN individuals.
2. **Interpretation**: Our findings suggest that NDAN individuals experience significant dendritic spine remodeling, primarily in areas distal to amyloid plaques. This might represent a compensatory mechanism to counteract the toxicity associated with AD pathology, potentially facilitating the turnover of mature dendritic spines to a more dynamic type.
3. **Future directions**: The results highlight the potential therapeutic value of fostering the transition from mature to immature and plastic synapses, with a particular focus on the role of Pin1. This insight could be pivotal in developing new approaches for synaptic rejuvenation in AD treatment, pointing to a promising direction for future research in synaptic plasticity and neuroprotection in AD.

Spines are distinct identifiable protuberances from dendritic shafts of postsynaptic neurons, primarily receiving excitatory signals that play a critical role in forming synaptic connections facilitating neuronal communication.[26,27] Changes in their structure and density are associated with a range of processes, from memory formation to the onset of neurodegenerative diseases.[28] Indeed, research has shown an association between Aβ plaque buildup and morphological changes in dendritic spines, with the latter leading to cognitive decline.[11,23,24,28,29] We extended our analysis to include the protein Peptidyl-prolyl cis-trans isomerase NIMA-interacting 1 (Pin1), identified as a potentially significant factor in this study. Pin1 is a protein associated with AD pathogenesis, with a crucial role in synaptic plasticity, especially within dendritic spines and shafts, where it regulates protein synthesis essential for maintaining the late phase of long-term potentiation.[30–32] Pin1 is critical in Aβ42-induced dendritic loss[30] and exhibits reduced levels in regions prone to AD and elevated levels in resilient areas, suggesting a link between its concentration and the brain region vulnerability.[33] We perform this study using frontal cortex, which is strongly affected by the AD pathology and presents a robust reduction of synaptic excitatory input documented in AD but not in NDAN.[21] To gain further insight into dendritic spine adaptability and Pin1 distribution, we analyzed the morphology, density, and distribution of dendritic spines in the frontal cortex areas adjacent to and away from the plaques.

TABLE 1 Clinical data of human subjects used in this study.

A. Alzheimer's Disease Center Sanders-Brown Center on Aging at the University of Kentucky (UK): DiI labeling					
Diagnostic	Age	Gender	MMSE	Braak stage	PMI (h)
CTRL	86	F	30	1	1.75
CTRL	85	F	30	2	3.1
CTRL	80	F	30	2	2.63
CTRL	83	F	30	2	1.83
AD	69	F	0	6	1.26
AD	60	M	9	6	17.33
AD	81	F	15	6	18
AD	72	M	8	6	12
NDAN	87	F	30	5	2.5
NDAN	94	F	30	4	3
NDAN	77	M	30	4	2.75
NDAN	87	F	30	4	2.25
B. Oregon Brain Bank at the Oregon Health and Science University (OHSU): Immunofluorescence and western blotting experiments					
Diagnostic	Age	Gender	MMSE	Braak stage	PMI (h)
CTRL	86	F	29	2	8
CTRL	83	M	29	1	<14
CTRL	74	F	29	2	7.5
CTRL	90	F	29	2	9
CTRL	100	F	29	2	2.5
AD	90	F	20	6	5
AD	87	F	N/A	6	2.5
AD	83	M	N/A	5	13
AD	88	M	N/A	6	4
AD	95	M	21	6	5
NDAN	93	M	26	4	4
NDAN	90	F	28	4	8
NDAN	82	M	28	4	8
NDAN	92	M	28	4	3 days
NDAN	98	F	27	4	4.75

Note: Braak stage: A measure of the number and location of tau tangles and Aβ plaques in the brain.
Abbreviations: MMSE, Mini-Mental State Examination (administered within the last year); PMI, *post mortem* interval.

2 | METHODS

2.1 | *Post mortem* human brain samples

Formalin-fixed *post mortem* human frontal cortices from four CTRL, four AD, and four NDAN individuals, aged 60 to 94 years with *post mortem* intervals (PMIs) ranging from 1 to 18 h (Table 1A), were sourced from the National Institute on Aging-funded University of Kentucky Alzheimer's Disease Research Center of the Sanders-Brown Center on Aging at the University of Kentucky (UK), USA, for DiI labeling. For immunofluorescence labeling, fresh frozen *post mortem* human frontal cortices from five CTRL, five AD, and five NDAN individuals, aged 74 to 100 years with PMIs ranging from 2 to 72 h (Table 1B), were procured from the Oregon Brain Bank at the Oregon Health and Science University (OHSU), Portland, OR, USA. Donors were clinically evaluated in studies at the National Institutes of Health (NIH)-sponsored Layton Aging and AD Center (ADC) at OHSU, as detailed in Fracassi et al.[25] Brain tissue collection took place at autopsy, with approvals from the Institutional Review Board. Pathological characteristics for AD, NDAN, and CTRL were ascertained using the Consortium to Establish a Registry for Alzheimer's Disease (CERAD) criteria and Braak's criterion. The cohort listed in Table 1A was used for DiI assay (Figures 1, 2, 3, and 4); the cohort listed in Table 1B was used for immunofluorescence and western blotting experiments (Figure 5).

2.2 | Tissue preparation

Upon arrival, the formalin-fixed cortex tissue blocks approximately sized 0.5 × 1 × 1 cm^3 designated for DiI labeling were processed and transferred to 0.1 M phosphate buffer saline (PBS), pH 7.4 (Catalog No. BP665-1, Fisher Scientific, Fair Lawn, NJ, USA). These tissue sections, each 100 μm thick, were processed on a vibratome either the day before or on the day of DiI labeling. Sections were stored in sterile 0.1 M PBS, pH 7.4 at 4°C until use. For immunofluorescence labeling, the fresh frozen cortex tissue blocks were thawed from −80°C, then cryoprotected using OCT compound (Catalog No. 4585, Fisher HealthCare, Houston, TX, USA), sectioned at 12 μm onto Superfrost/Plus slides (Catalog No. 12-550-15, Fisherbrand, Fisher Scientific, Pittsburgh, PA, USA). Prepared slides were stored at −80°C until use.

2.3 | Neuronal structure labeling

The neuronal structures underwent labeling using the lipophilic dye, DiI, 1,1′-dioctadecyl-3,3,3′,3′-tetramethylindocarbocyanine perchlorate (Catalog No. D282; Invitrogen, Eugene, OR, USA). DiI was sonicated for at least 4 h until it turned into fine crystals. A fine crystal was picked using a 30-gauge needle and gently applied to a moist tissue section in 0.1 M PBS, pH 7.4, under a dissection microscope. After incubation for 72 h at 4°C, DiI-stained tissue sections were fixed with 4% paraformaldehyde for 5 min. The sections then underwent three 8-min washes in 0.1 M PBS, pH 7.4 at room temperature (RT). To enhance the visualization of amyloid plaques, sections were incubated in 2 μg/mL Thioflavin S (Thio-s) for 8 min followed by three 3-min washes in 0.1 M PBS, pH 7.4. Subsequently, sections were treated with TrueBlack Plus lipofuscin autofluorescence quencher (Catalog No. 23014, Biotium, Fremont, CA, USA) for 7 min, rinsed with 0.1 M PBS, pH 7.4, to remove excess and mounted on glass slides with Prolong Glass hard set mounting medium (Figure 1A).

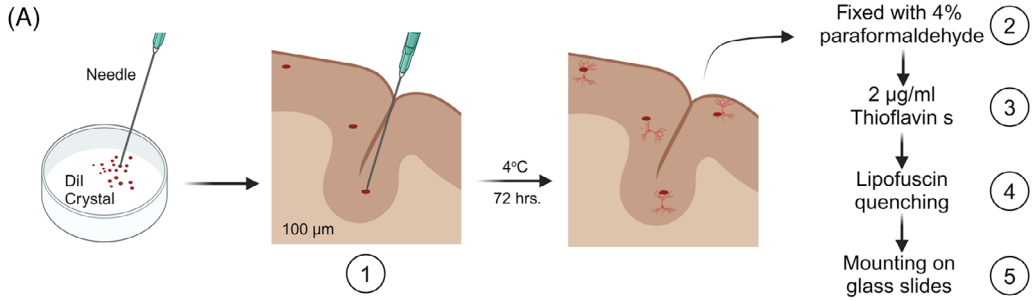

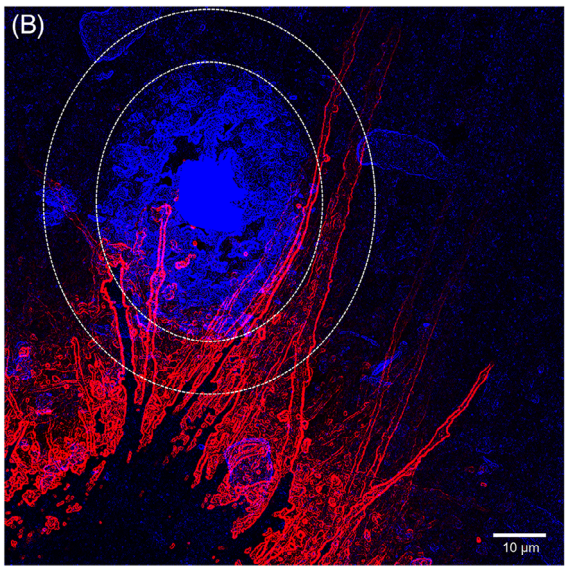

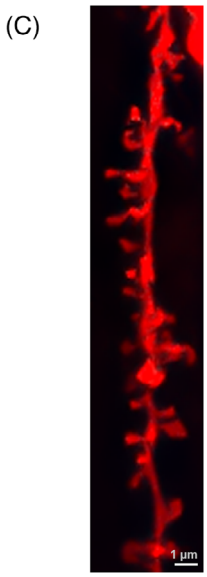

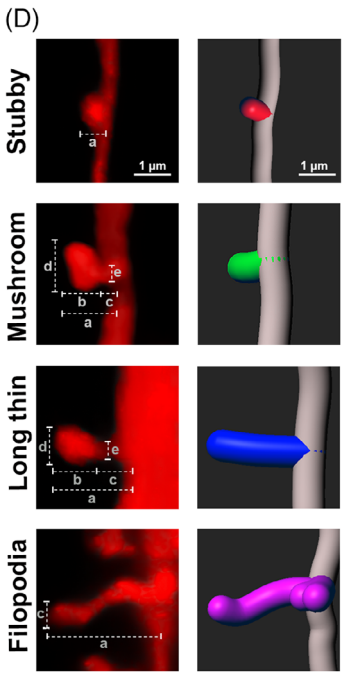

Spine Dimensions	
a	Total spine length
b	Spine head length
c	Spine neck length
d	Spine head width
e	Spine head width

(E)

Spine Types Criteria	
Stubby	Length (spine) < 1 µm
Mushroom	Length (spine) < 3 µm Maximum width (head) > mean width (neck) x 2
Long Thin	Mean width (head) ≥ mean width (neck)
Filopodia/Other	None

FIGURE 1 Illustration of DiI labeling steps of neuronal structure in *post mortem* human frontal cortex and analysis of dendrites and spine parameters. (A) Simplified steps of DiI application on brain tissue sections and thioflavin labeling. (B) Representative picture of dendrites (red) surrounding the Aβ plaque (blue in a small oval). The area defined as proximal to the plaque includes Aβ plaque and the surrounding 10-μm area. The area outside the large oval without plaque deposition is considered distal area. (C, D) Image of dendrite (C) and 3D reconstructions of the different types of spine (D) after analysis using Filament tracer and Classify Spines XTension Imaris analysis software version 9.9. Dendrite length, dendrite diameter, spine number, spine density, and dendritic spine morphology in the proximal area versus distal area were analyzed. (E) Spine classification criteria according to Classify Spines XTension Imaris analysis software version 9.9. Donor information described in Table 1A.

2.4 | Immunofluorescence

The fresh frozen *post mortem* human frontal cortices sections were fixed in 4% paraformaldehyde for 30 min and washed three times in 0.1 M PBS, pH 7.4, each for 7 min. Sections were then incubated for 1 h at RT in a blocking buffer solution containing 10% Normal Goat Serum (NGS), 5% bovine serum albumin, 0.5% Triton-x100, and 0.05% Tween 20 in 0.1 M PBS, pH 7.4. The sections were then exposed overnight to a 1:200 solution of rabbit-anti-Pin1 primary antibody (Catalog No. 10495-1-AP, Proteintech, Rosemont, IL, USA) in 0.1 M PBS, pH 7.4, with 1.5% NGS. On a subsequent day, after three 8-min washes in 0.1 M PBS, pH 7.4, sections were incubated in a 1:400 solution of goat-anti-rabbit Alexa Flour 488 secondary antibody (Catalog No. A1108, Invitrogen, Eugene, OR, USA) with 1.5% NGS in 0.1 M PBS, pH 7.4, for 1 h at RT. After three 8-min washes in 0.1 M PBS, pH 7.4, sections were exposed to 2 μL/mL Thio-S in 0.1 M PBS, pH 7.4, for 8 min, washed three times for 3 min each in 0.1 M PBS, pH 7.4, then mounted using EverBrite TrueBlack hardset mounting medium enhanced with far-red NucSpot 640 (NucS 640, Catalog No. 23019, Biotium, Fremont, CA, USA) and stored at 4°C.

2.5 | Imaging

Images of DiI-labeled dendrites in gray matter, both proximal and distal to the Aβ plaques, were captured within 3 days. An Olympus FV 3000 Laser Scanning Confocal microscope was employed, with laser excitations at 405 and 559 nm to visualize Thioflavin S and DiI, respectively. Each image was viewed under a 63× immersion oil objective. Images with a resolution of 800 × 800 pixels, composed of stacks of 70 images at dimensions of 0.132 x 0.132 x 0.28 μm per step, with a zoom of 2, were used to generate a three-dimensional construct of dendrite structures. Similarly, z-stack images illustrating Pin1 distribution near and distant from the plaque were captured using a Keyence BZ-X800 (Keyence Corporation) with a 60× immersion oil objective. These images had a resolution of 1920 × 1440 pixels, with 15-image stacks at a z-step size of 1 μm.

2.6 | Image analysis

Filament Tracer module and Classify Spines XTension (https://imaris.oxinst.com/open/view/classify-spines) tools in the Imaris analysis software version 9.9 were used for quantitative analysis of dendrites and spine classification. For dendritic spine quantification, analysis was focused on areas both proximal and distal to the plaques. The dendrite of interest (DOI) is defined as unbranching and/or non-overlapping with any other dendrite segment. Dendrite segments ranging from 10 to 50 μm in length, either passing through the Aβ plaque or located within a 10-μm radius around it, were categorized as belonging to the proximal region. Dendritic segments within the same length range but situated in areas devoid of plaques or distant from the proximal region were labeled as part of the distal region (Figure 1B,C). Three images of neurites were captured in the proximal area, and three were taken in the distal area for each section. For each subject, three sections were analyzed, and one to four dendrites from each image were examined. The Filament Tracer module and the Classify Spines XTension were employed to visualize and measure various parameters, including dendrite length (ranging from 10 to 50 μm), dendritic diameter, dendritic spine morphology, and spine density in both the proximal and distal regions relative to the plaque. Dendritic spine density was defined as the number of spines per 10-μm length of dendrite. In the surpass mode of the Filament Tracer module, dendrite segments and spines were traced using the autopath algorithm, resulting in a tree-like filament structure based on local intensity contrast. Dendritic spines were measured in three dimensions. The maximum diameter of dendrites was constrained to 6 μm, and the minimum diameter for spines was set at 0.26 μm. Automatic thresholds were applied to generate spine seed points and for surface rendering. Following the trace generation, a filter was applied to ensure precise identification of all dendritic protrusions as spines. The classification of the different types of spines was assessed based on criteria pre-established by the Classify Spines Xtension software. Briefly, the classification rules combine the spine morphology categories (Spine, Head, Neck, Ground) with the following variables: volume, length, mean/ minimum/ maximum/ width. Each class is identified by name, classification rule, and color (Figure 1D,E).

Spine classification was based on predefined criteria established by the Classify Spines XTension software, categorizing spines into four classes: (i) Stubby spines were defined by a length of less than 1 μm. (ii) Mushroom spines exhibited a length less than 3 μm, with the maximum width of the spine head being at least twice the mean width of the spine neck. (iii) Long thin spines were characterized by a mean width of the spine head equal to or greater than the mean width of the spine neck. (iv) Filopodia/other included dendrites and spines not falling into the previous categories (Figure 1D). These predefined criteria generate a binary output, where 1 signifies true and 0 denotes false. The total number of spines within each class was computed by summing the results of these predefined criteria. Then, spines falling into class iv, filopodia/other, were subjected to more stringent criteria of selection and classification: a head diameter less than 0.35 μm, a head-to-length ratio greater than 2.5, and a head-to-neck ratio less than 1.1 μm, resulting in their reclassification as filopodia.[34] Considering long thin and filopodia are indicative of immature, less stable spines with the potential to transition into different types of spines[35] or undergo extension and retraction processes, we chose not to impose constraints on the spine length. Table 2 shows the geometric measurements of dendritic spine morphology, independent of subject group and location. For the quantitative analysis of Pin1, a total of three or four sections per subject were examined. For each section, 10 images were captured: five images of Pin1 surrounding a plaque of similar size and five images of Pin1 in areas free of plaques. ImageJ software (https://imagej.nih.gov/ij, NIH) was utilized for the quantitative analysis of the Pin1 fluorescence marker. Fluorescence intensity was measured, and the sum of the pixel values in a region of interest (ROI) was expressed as integrated

TABLE 2 Geometric measurements of dendritic spine morphology, independent of subject group and location.

	Stubby	Mushroom	Long Thin	Filopodia	Total
Length	0.57 ± 0.44	1.46 ± 0.43	2.02 ± 0.97	1.69 ± 1.11	0.85 ± 0.72
Neck width	0.09 ± 0.27	0.40 ± 0.65	0.71 ± 0.48	0.40 ± 0.07	0.2 ± 0.42
Head width	1.04 ± 0.55	1.75 ± 0.95	1.06 ± 0.77	0.31 ± 0.03	1.08 ± 0.68

Note: Filopodia were categorized separately from the rest of the spines under category iv (Filopodia/Other). Mean values are presented with their corresponding standard deviations. Values are expressed in μm.

density (IntDen), using the following formula: IntDen = Area × Mean gray value.

2.7 | Western blotting

Frontal cortex tissue (25 mg) from age-matched controls ($n = 6$) and AD and NDAN subjects ($n = 7$/group) were homogenized on ice in 1× RIPA buffer (#9806, Cell Signaling Technology Inc., Danvers, MA, USA) containing 1 mM PMSF, 1× Halt Protease and Phosphatase Inhibitor Cocktail (Thermo Fisher Scientific, Rockford, IL, USA). Tissue lysates were centrifuged for 15 min at 15,000 × g, 4°C. Protein concentrations were measured using the Bio-Rad protein assay kit (Bio-Rad Laboratories, Inc., Hercules, CA, USA).

Protein lysates (15 μg) were resolved by 4% to 15% SDS-PAGE (Criterion TGX, Bio-Rad Laboratories, Inc., Hercules, CA, USA), electrophoretically transferred to polyvinylidene difluoride membranes (Immobilon-P, Millipore, Billerica, MA, USA), and subjected to immunoblotting analysis. Protein blot membrane was blocked in 3% bovine serum albumin and Tris-buffered saline (TBS)/0.1% Tween-20 (TBS-T) for 1 h at RT. Antibodies used were as follows: anti-Pin1 (1:1000, Catalog No. 10495-1-AP, Proteintech, Rosemont, IL, USA) overnight at 4°C, anti-β-actin (1:50000, Catalog No. A1978, Sigma-Aldrich, St. Louis, MO, USA) for 1 h at RT. HRP-conjugated secondary antibodies were used: anti-rabbit IgG (1:5000, Catalog No. 7074, Cell Signaling Technology), anti-mouse IgG (1:5000, Catalog No. 7076, Cell Signaling Technology) for 1 h at RT. Signal detection was performed with Electrochemiluminescence Western Blotting Detection Reagents (RPN2209, Cytiva Amersham, Marlboroug, MA, USA). Expression levels were evaluated by quantification of the relative density of each band normalized to that of the corresponding β-actin band density, using ImageJ software version 1.46r (NIH, Bethesda, MD, USA). Results were graphed using GraphPad Prism 9 (San Diego, CA, USA). One-way ANOVA followed by Tukey's comparison test was used to determine significance at $p < .05$.

2.8 | Statistical analyses

For the dendritic spine study, statistical tests were performed using GraphPad Prism software version 9.5.1. Where appropriate, one-way ANOVA or two-way ANOVA followed by Tukey's multiple-comparisons tests were used to detect statistical significance between and within groups. Pearson's correlation coefficients were used to examine the relationship between age or PMI and number of spines, spine density, dendritic diameter, and dendritic spine morphologies. Data were presented as mean ± SD, and $p < .05$ was considered statistically significant.

We calculated the total number of spines (stubby, mushroom, long thin, and filopodia) both proximally and distally to the plaques in CTRL, AD, and NDAN subjects. Then, considering only the spines in the proximal area to the plaques, we proceeded as follows: we computed the total number of spines (stubby, mushroom, long thin, and filopodia) within each diagnosis. For each type of spine, we used a chi-squared test to determine whether the percentage of that type of spine differed between diagnoses. We also carried out a chi-squared test to determine whether the overall distribution of spine types differed between diagnoses. The same analysis was then repeated for spines located in the distal area. Within the CTRL group we proceeded as follows. We computed the total number of spines (stubby, mushroom, long thin, and filopodia), both proximally and distally to plaques. For each type of spine, we used a chi-squared test to determine whether the percentage of that type of spine differed between distances. We also carried out a chi-squared test to determine whether the overall distribution of spine types differed in relation to distance from the plaques (distal area vs proximal area plaque). This analysis was repeated for AD and NDAN subjects. Within the proximal area spines, we examined stubby percentage, stubby per 10 μm, mushroom percentage, mushroom per 10 μm, long thin percentage, long thin per 10 μm, filopodia percentage, and filopodia per 10 μm. We carried out an ANOVA to detect differences between diagnoses. We repeated the ANOVA with a random effect for the individual subjects from which samples came. The same analysis was then repeated for distant spines. All analyses were conducted using R Statistical Software version 4.2.2 (R Core Team 2022). R Core Team, "R: A language and environment for statistical computing" (R Foundation for Statistical Computing, Vienna, Austria, 2022).

3 | RESULTS

3.1 | Differential dendritic morphology in areas proximal and distal to Aβ plaques in AD versus NDAN

Considering the pivotal role of Aβ oligomers in causing the loss of dendritic spines and the morphological alterations linked to synaptic dysfunction in individuals with AD,[28,36–38] we conducted a comparative histological study of dendrites and dendritic spines in the frontal

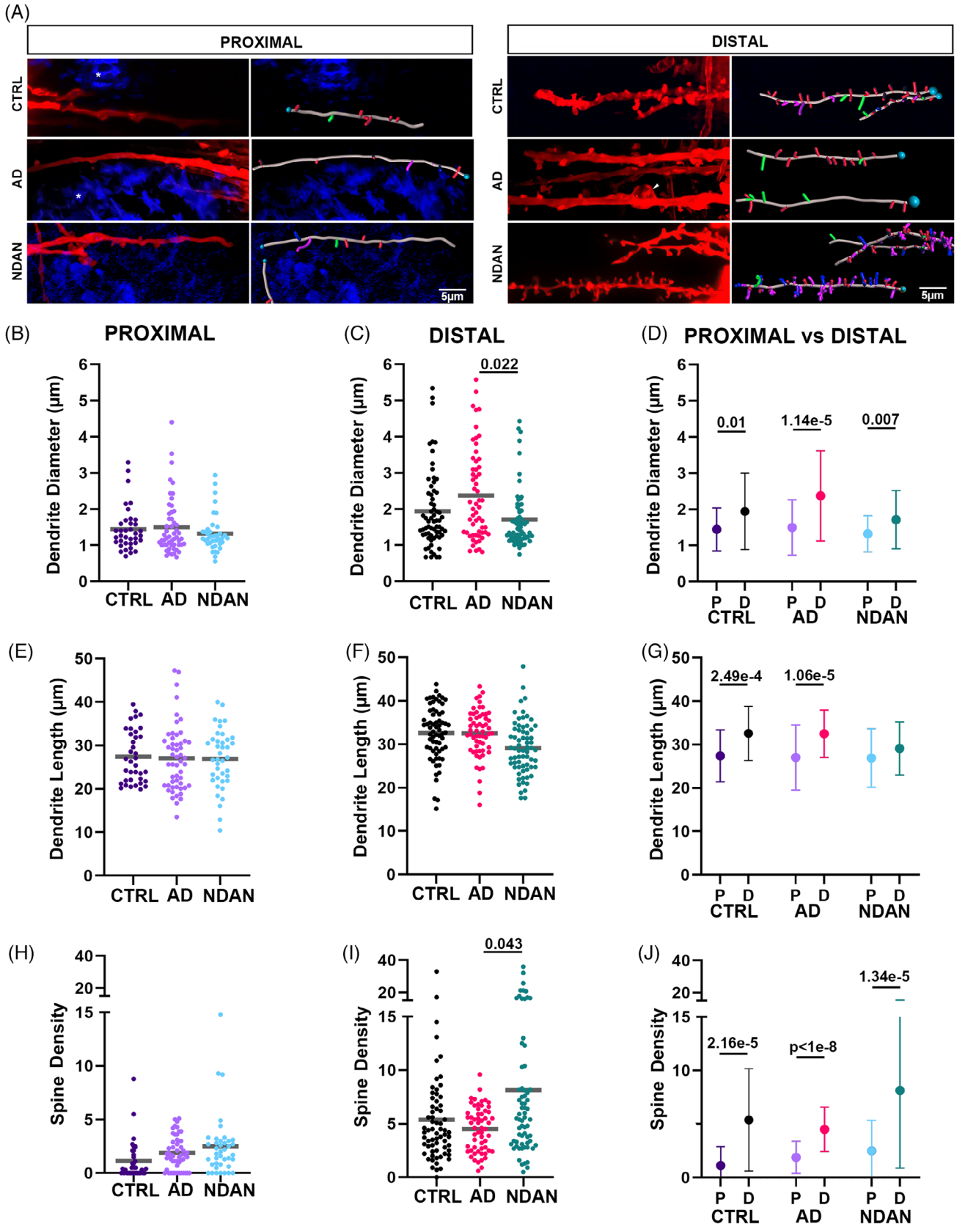

FIGURE 2 Quantitative analysis of dendrite diameter, length, and total spine density. Proximal (A) and distal (B) dendrites and their dendritic spines shown in red. A white asterisk highlights an amyloid plaque. An arrowhead points to a bulbous dilation of a dendrite observed in the frontal cortex of an AD *post mortem* brain sample. The respective right columns present reconstructed 3D images of the dendritic spines and dendrites, based on the images in the left columns. Turquoise circles indicate the starting points of each quantified dendrite. Stick-like shapes are color coded:

cortex of age-matched CTRL, AD, and NDAN individuals. We stained Aβ plaques using thioflavin and selected as a proximal area the region within 100 μm of the plaques and a distal area farther than 100 μm (Figure 1). DiI-labeled dendrites and 3D image reconstruction revealed that CTRL, AD, and NDAN groups showed a significant reduction in dendrite diameter (Figure 2A–D), dendrite length (Figure 2A,E–G), and spine density (Figure 2A,H–J) in the proximity of the plaques compared to the distal area (Figure 2D,G,J), except for the dendrite length in the NDAN group (Figure 2G). Interestingly, we found no differences within groups in the proximal area concerning dendrite diameter, dendrite length, and spine density (Figure 2A,B,E,H), indicating a uniformly toxic environment across all groups. Nonetheless, in the distal region, the AD group displayed enlarged dendrites in comparison to the NDAN group (Figure 2A, white arrow), indicating the presence of swollen and compromised dendrites even at a distance from the plaques. A comparable trend emerged from a quantitative analysis comparing the diameters of AD dendrites with those of CTRL and NDAN, with the latter showing a significant reduction in diameter (Figure 2C). Meanwhile, the dendrite length in the distal area showed no significant differences among the groups (Figure 2F). Notably, far from plaques, the NDAN group showed a higher spine density compared to the AD group, with a similar trend compared to the CTRL subjects (Figure 2I). This result suggests that NDAN individuals may possess a compensatory response that is absent in AD patients, resulting in the preservation or increase in dendritic spine numbers in regions characterized by a less toxic environment.

3.2 | NDAN individuals have increased density of highly dynamic spines

Because dendritic spine types and their morphology change in response to certain stimuli or stress conditions,[39–42] we examined the distribution of different dendritic spine types across the three study groups. Briefly, filopodia are dynamic structures capable of transitioning into various types of spines. They are characterized by their long, slender shape, lacking a distinctive head.[43–45] Long thin spines, characterized by small heads and elongated necks, are thought to play a role in learning and can evolve into mushroom spines over time.[43,44] Stubby spines, identified by short, wide necks and the absence of a distinct head, may represent an intermediate stage, potentially forming after the degeneration of mushroom spines.[43,44,46] Finally, mushroom spines, considered mature synapses due to their stable and enduring structure, are associated with long-term memory consolidation.[43,44,47]

We assessed the density of each spine type in proximity to and at a distance from plaques. First, we analyzed the different types of dendritic spines in the proximal area, and we found no differences among the groups for each of the analyzed types (Figure 3A,D,G,J). Interesting findings were made in the distal area, where our analyses showed that AD individuals were characterized by a reduced density of stubby, long thin, and filopodia/other spines compared to NDAN (Figure 3B,H,K). Notably, the levels of stubby, long thin, and filopodia/other spines did not change between CTRL and AD. However, the density of mushroom spines in AD was significantly higher than NDAN (Figure 3E). Moreover, when filopodia spines were separated from the filopodia/other group using the more stringent criteria (see method section *Image analysis*), we observed filopodia spines only in the NDAN group, specifically a larger number of filopodia spines were observed in the distal area compared to the proximal area. However, this difference was not statistically significant. Notably, filopodia were absent in both the AD and CTRL groups. Overall, our analysis showed that, for most spine types (Figure 3C,F,I,L), the densities were higher in the distal than in the proximal area across all groups. Exceptions to this pattern were the mushroom spines in the NDAN group (Figure 3F), long thin spines in the AD group (Figure 3I), and filopodia/other in the CTRL group (Figure 3L). This disparity in spine type density prompted us to examine whether the percentage distribution of spine types varied among diagnostic groups, in both the proximal and distal areas. We observed that stubby spines were predominant among all spine subtypes, irrespective of group or location, constituting the highest percentage compared to other spine types. Conversely, in NDAN individuals, mushroom spines were the least prevalent (Figure 4A,B). Notably, in contrast to NDAN, long thin spines were the least common in both AD and CTRL in both regions. Furthermore, examining the percentage distribution within both the proximal and distal areas, we determined that in the proximal area, the prevalence of mushroom spines significantly varied among diagnostic groups. In contrast, in the distal area, the variation was more pronounced across all spine types and all groups (Figure 4C).

We also conducted a statistical analysis on other spine parameters, performed independently of the categorization of spine types in which we analyzed length, area, and volume (Figure S1). Our findings indicate that in regions both proximal and distal to plaques, AD subjects exhibited significantly larger dendritic spines, specifically greater area and volume, in contrast to NDAN subjects, who presented the smallest spine dimensions.

3.3 | Different Pin1 distribution and increased expression in NDAN and CTRL as compared to AD

The modulation of spine morphology, spine density, and synaptic function by Pin1 proteins has been previously documented,[32] as has its impact in synaptic plasticity in AD.[48] We tested the hypothesis that the

red for stubby spines, green for mushroom spines, blue for long thin spines, magenta for filopodia. No significant differences were identified in the Aβ plaque proximity: dendrite diameter (B), length (E), or total spine density (H) among CTRL, AD, and NDAN. (C) In the distal area, AD individuals showed larger dendrite diameter compared to NDAN. The dendrite length (F) in the distal area was not different among the groups. (I) Total spine density was higher in NDAN compared to AD, in the distal area. When comparing the proximal area to the distal area, the dendrite diameter (D), length (G), and total spine density (J) in the distal area exceeded those in the proximal area for all groups, except for the dendrite length of NDAN. For statistical tests, we used a mixed-effects ANOVA model with a random intercept for the individuals. Donor information described in Table 1A.

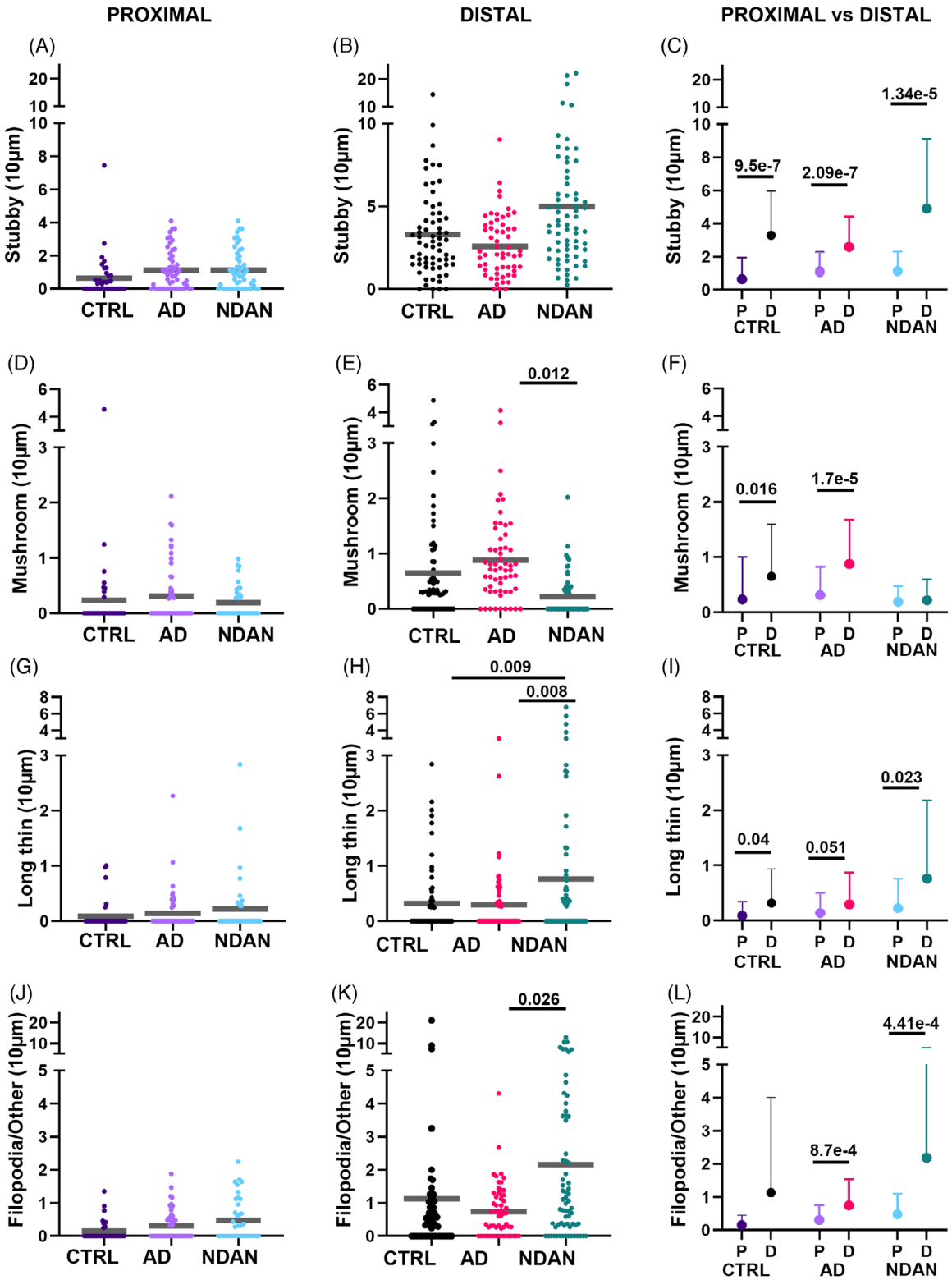

FIGURE 3 Quantitative analysis of spine types relative to Aβ plaques. Stubby spines (A–C), mushroom spines (D–F), long thin spines (G–I), and filopodia (J–L) were analyzed expressed as number of spines per 10 μm, in proximity and distally to the Aβ plaques. There were no significant differences in spine density of stubby (A), mushroom (D), long thin (G), or filopodial (L) between CTRL, AD, and NDAN in the proximal area. In the distal area: (B) Stubby spines did not show differences within groups; however, (E) AD subjects have significantly higher levels of mushroom spines compared to NDAN. In the distal area, (H) long thin spine density was higher in NDAN compared to CTRL and AD individuals, and filopodia (K) spines were higher in NDAN compared to AD. The densities of the four spine subtypes (C, F, I, L) were higher in distal areas than in the proximal area, except for mushroom spines in NDAN (F), long thin in AD (I), and filopodia in CTRL (L). For statistical tests, we used a mixed-effects ANOVA model with a random intercept for the individuals. Donor information is presented in Table 1A.

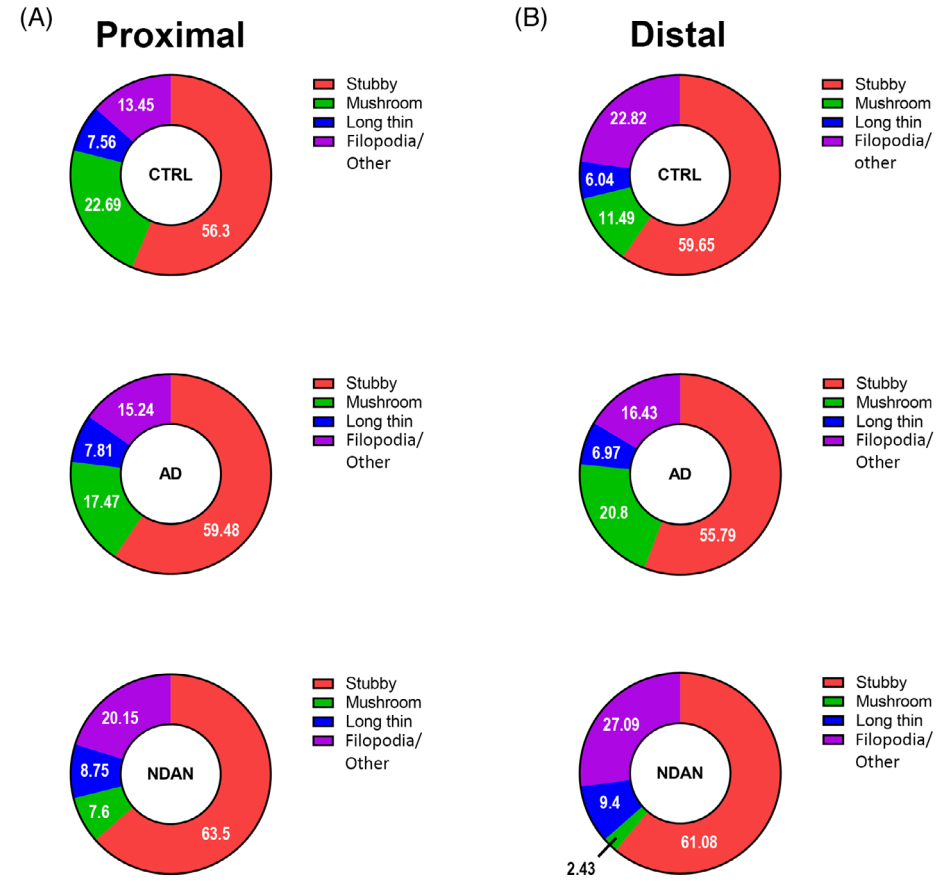

(C)

	Proximal	Distal
Spine types	***p* value**	***p* value**
Stubby	.37083	.0391
Mushroom	1e-4	<1e-8
Long thin	.89505	.00283
Filopodia	.17212	<1e-8

FIGURE 4 Percentage of spine subtypes relative to Aβ plaques. Donut diagrams showing CTRL, AD, and NDAN spine subtype relative abundances expressed in percentages, in proximal (A) and in distal (B) areas. Spine subtypes are color coded: red for stubby spines, magenta for filopodia spines, blue for long thin spines, and green for mushroom spines. In the distal area, the densities of stubby, mushroom, long thin, and filopodia spines differ significantly between CTRL, AD, and NDAN. In contrast, in the proximal area, the spine densities of all types, except for the mushroom spines, did not show significant differences (see *p* values in (C). For statistical analysis, a chi-squared test was used to determine whether the percentage spines differed between diagnoses (C). Donor information is presented in Table 1A.

changes observed in dendritic morphology and spine densities were associated with a different distribution of Pin1 (Figure 5). To evaluate Pin1 distribution, we used an antibody specifically designed to mark Pin1 in the frontal cortex gray matter of CTRL, AD, and NDAN samples. Microscopic observations in the proximal area revealed that all the groups showed Pin1 localized within the plaque and appeared as clusters in the vicinity of the nuclei (Figure 5A). In contrast, in regions farther from the plaques, Pin1 localization differed among groups. In AD samples, Pin1 was mainly seen in the neuronal soma (Figure 5B). Conversely, in both NDAN and CTRL samples, Pin1 was evenly distributed between cell processes and soma, as shown in Figure 5B. Quantitative analysis of immunoreacted sections indicated that Pin1 protein distribution was significantly higher in the distal area compared to the proximal area (Figure 5B,D,E) in NDAN and CTRL, but not in AD samples. In the area close to plaques, Pin1 expression was higher in NDAN compared to CTRL and AD samples (Figure 5A,C,E). Investigating the association between Pin1 expression and AD progression, we conducted a Pearson's correlation analysis. Pin1 levels, quantified through immunofluorescence (IF) by aggregating proximal and distal measurements, demonstrated a significant correlation with both cognitive impairments, as assessed by Mini-Mental State Examination (MMSE), and neuropathological severity, indicated by Braak

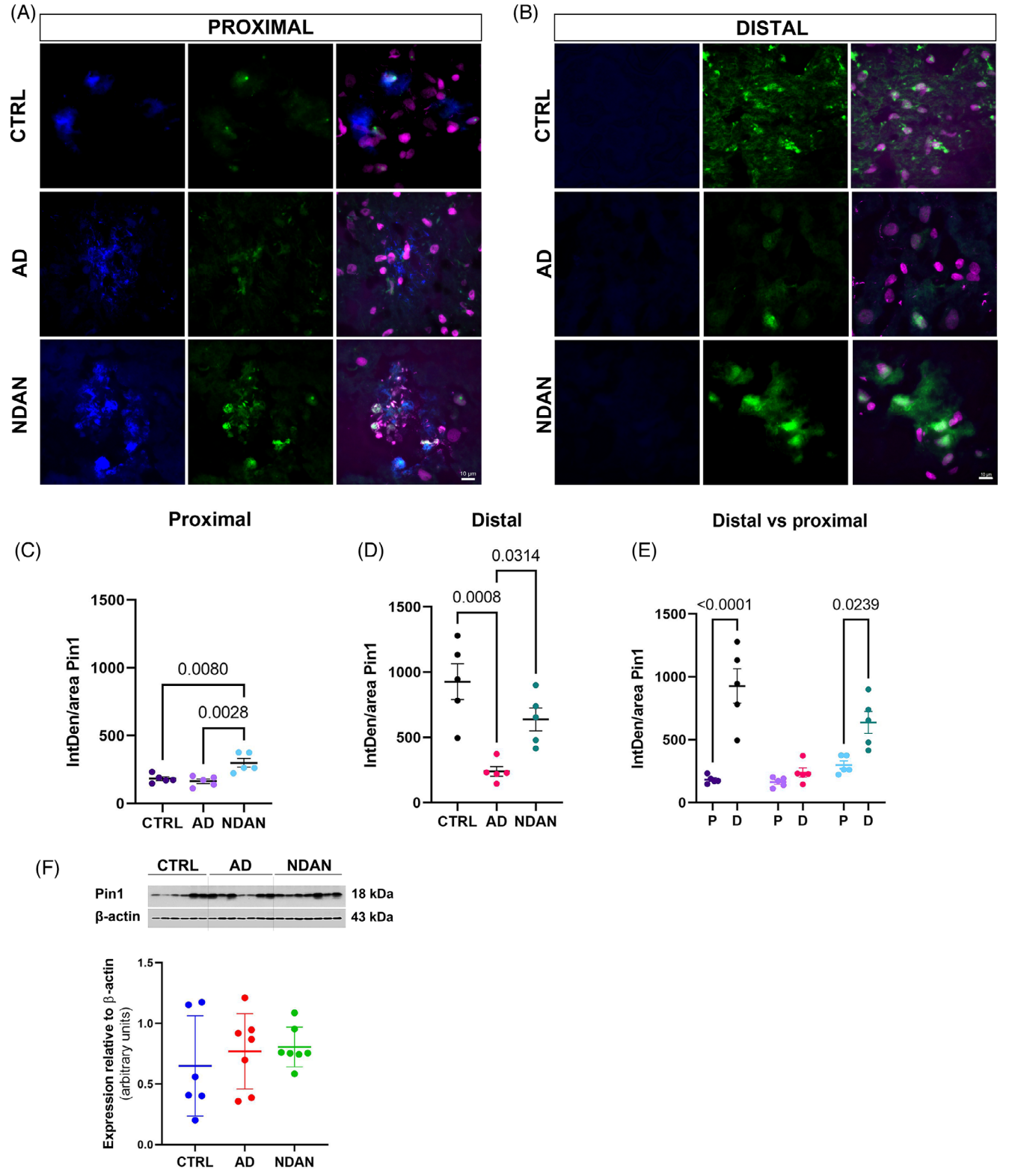

FIGURE 5 Levels of Pin1 relative to Aβ plaques. (A, B) Representative images displaying Pin1 distribution in the proximal area compared to the distal area in CTRL, NDAN, and AD subjects. (C) Integrated density of Pin1 distribution showed higher levels of this protein in NDAN compared to AD and CTRL, close to the plaque. (D) Distal to plaques, AD showed significantly lower levels of Pin1. (E) NDAN and CTRL showed higher levels of Pin1 in distal regions compared to proximal; this difference was not observed in AD individuals. (F) Western blot analysis of Pin1 protein expression relative to β-actin did not show differences within groups. For statistical analysis, one-way ANOVA was used, followed by Tukey's multiple-comparisons test, $p < .05$. Value is expressed as mean ± SD. Donor information is presented in Table 1B.

staging (Figure S2A,B). To ensure that the variations in the PMI did not affect the measurements, we also performed a correlation analysis between PMI values and IF results presented here using a Pearson's correlation test. No correlation was found between PMI values and any of the elements/antigens studied here. Therefore, observed differences could not be attributed to differences in non-specific *post mortem* tissue degradation. The same held true when we correlated IF values with ages (Figure S2C,D). Additionally, western blot assessments of total protein lysates from the frontal cortex indicated no statistically significant differences among the groups (Figure 5F).

4 | DISCUSSION

The aim of this work was to explore potential synaptic differences associated with cognitive resilience by examining dendritic spine morphology and their integrity in relation to Aβ plaques in CTRL, AD, and NDAN individuals. Specifically, our goal was to shed light on the possible synaptic contributions underlying cognitive resilience, peculiar to NDAN subjects.

As previously described, NDAN individuals are distinguished by a unique microglial phenotype, specifically localized near Aβ plaques. These microglia, characterized by heightened TREM2 expression and increased phagocytic activity, appear to be actively involved in clearing damaged synapses. This specialized microglial subset is thought to play a protective role in preventing extensive damage along axons and dendrites.[25] Therefore, the presence of this microglial population suggests the existence of a synaptic recycling mechanism, wherein compromised mature synapses are engulfed and subsequently replaced by newly formed synapses. Based on these premises, we hypothesized that this process likely contributes to synaptic resilience and plasticity within the brains of NDAN individuals, ultimately contributing to cognitive integrity, through the preservation and remodeling of dendritic spines. To test this hypothesis, we focused on the frontal cortex as our area of investigation. This region has been studied, and it exhibits significant synaptic excitatory input remodeling in AD but not in NDAN individuals.[21] Moreover, the frontal cortex is integral to the default mode network, a resting-state network linked with self-referential cognitive processes like introspection and autobiographic memory, that is significantly affected in AD individuals.[49,50]

Consistent with previous studies in AD[51–53] and animal models[37,54] that have shown synaptic and spine loss near plaques, we observed in all groups a decrease in dendritic spine numbers near Aβ plaques, including in the CTRL group, suggesting that Aβ induced severe synaptic toxicity.[36,37,55,56] NDAN individuals, as opposed to those vulnerable to AD, appear to counteract this toxicity in regions distant from the plaques, as indicated by the augmented spine density. These findings imply that in resilient individuals, Aβ toxicity is confined to the immediate proximity to plaques. In AD patients, analysis of Aβ distal dendrites revealed increased dendrite diameter compared to NDAN subjects. This was confirmed by further analyses conducted on spines' length, area, and volume indicating that in regions both proximal and distal to plaques, AD subjects exhibited significantly larger dendritic spines. In light of our recent study revealing reduced autophagy in AD and preserved in NDAN individuals, we hypothesize that enlargement of the dendritic diameters may indicate a stressed autophagic process, resulting in the accumulation of partially digested cellular matter due to disrupted autophagosome-lysosome fusion.[20] NDAN subjects exhibit an increase of spine density in regions distant from plaques compared to both AD patients and CTRL individuals. This suggests the existence of potential compensatory mechanisms that counter dendritic loss near Aβ plaques, unlike in AD, where such mechanisms are absent. This difference could contribute to an augmented capacity for synaptic connection plasticity in NDAN individuals, potentially preserving their cognitive function.

We also conducted an analysis of dendritic spine types in CTRL, AD, and NDAN groups. Spine types were categorized based on phenotypic characteristics, ranging from the most dynamic and plastic to the least: filopodia, long thin, stubby, and mushroom. As described in the results section, dendritic spines are classified into four main types with distinct morphologies and functions: the stubby, which are short and immature; the mushroom, which are mature and stable; the thin, which are flexible and transient; and the filopodia, which are highly dynamic protrusions that actively explore the surrounding environment to form new synaptic connections.[43,57]

Our analysis indicated that in the proximal region, Aβ had a significant impact on dendritic spines by causing substantial reductions in all types of spines, possibly due to the disassembly of F-actin in dendritic spines described in this study.[58] Importantly, these reductions showed no significant differences among the studied groups. Notably, compared to AD, NDAN samples showed a significant decrease in mushroom spines and an increase in more immature spines in the distal area. NDAN subjects exhibited a higher density of transitional spines, such as long thin and filopodia, and showed a similar trend for stubby spines, in comparison with the more stable mushroom spines in the distal area. NDAN subjects exhibited a higher density of transitional spines, such as long thin and filopodia, and showed a similar trend for stubby spines, in comparison to the more stable mushroom spines in the distal area. This indicates a promotion of turnover from mature synaptic spines to more plastic and immature ones.

Dendritic spine rearrangement in select individuals may be attributable to the active involvement of glial cells. Microglia, by identifying and phagocytizing dysfunctional synapses, are instrumental in the maturation and remodeling of dendritic spine networks.[53] Astrocytes, by forming tripartite complexes with presynaptic and postsynaptic structures, play a pivotal role in regulating synaptic transmission and plasticity.[59] Notably, astrocytes appear to preferentially interact with larger dendritic spines,[60] suggesting a bias toward mushroom spines over more immature spine types. Head spine size correlates positively with the probability of neurotransmitter release and the size of the postsynaptic response[61,62] and, for AD subjects having larger numbers of mushroom spines compared to other types, may help to explain the typical circuit hyperexcitability found in AD individuals.[63,64] However, we know the limitations of certain speculation due to the fact that our sample was a post mortem fixed tissue. In addition, it has been shown that NDAN individuals exhibit

better preservation of astrocytes[19] and more microglia of a phagocytic phenotype[25] compared to AD individuals, ultimately making strong the case of a critical role of those cell types in maintaining synaptic health and cognitive integrity.

Upon identifying Pin1 as a potential key player in this protective mechanism through an extensive literature review, we subsequently focused our research on examining its expression levels and distribution. Pin1 is implicated in the regulation of dendritic spine formation and maintenance, influencing synaptic plasticity.[32,65] It also affects the conformational state of tau, a protein not only linked to AD pathogenesis but also essential for maintaining the cytoskeletal structure within dendritic spines.[66,67] Pin1 plays a critical role in Aβ42-calcineurin signaling, which ultimately leads to synaptic loss,[30] and the inhibition of calcineurin has been associated with a reduced incidence of AD.[68,69] Pin1 may also alter the processing of amyloid precursor protein (APP), influencing Aβ production.[70] In addition, Pin1 plays a critical role in neuroinflammation, potentially influencing the phenotype of microglia.[33] In our study we observed lower levels of Pin1 in AD compared to CTRL and NDAN, both distal and proximal to plaques. In addition, Pin1 levels correlated with cognitive score of the individuals (MMSE) and stage of the pathology (Braak stage). This suggests that the reduced expression of Pin1 in AD may contribute to the compromised synaptic integrity and plasticity observed in these individuals, highlighting its role in synaptic resilience mechanisms, as witnessed by high levels of Pin1 in NDAN individuals.

Overall, our research elucidates distinct patterns of dendritic spine morphology between vulnerable AD patients and resilient NDAN individuals. The increased spine density and immature spine types in NDAN individuals highlight a unique synaptic adaptability, which may play a key role in preserving cognitive function despite the presence of AD pathology. In addition, our findings indicate that the differential expression of Pin1 in NDAN individuals compared to those with AD may underpin a protective mechanism against synaptic damage and cognitive decline. This adds a new dimension to our understanding of AD pathogenesis and cognitive resilience, opening venues for exploring therapeutic strategies targeting Pin1-related pathways to promote synaptic welfare and potentially mitigate cognitive symptoms of AD.

AUTHOR CONTRIBUTIONS

Anna Fracassi, Jutatip Guptarak, and Pietro Scaduto made substantial contributions to the design of the study and prepared a draft of the manuscript. Morphological experiments were performed by Jutatip Guptarak. Western blotting experiments were performed by Batbayar Tumurbaatar and Wen Ru Zhang. Statistical analyses were conducted by Pietro Scaduto and Daniel Jupiter. Anna Fracassi and Giulio Taglialatela conceived, designed, and funded the study and gave final approval of the version published. All authors read and approved the final manuscript.

ACKNOWLEDGMENTS

We are thankful to Dr. Randall Woltjer from the Oregon Brain Bank at Oregon Health and Science University (OHSU) and to Dr. Peter Nelson from the Alzheimer's Disease Center, Sanders-Brown Center on Aging at the University of Kentucky for providing *post mortem* human brain samples needed for the study. The work was supported by the National Institutes of Health-National Institute on Aging (NIH/NIA) grant R21AG082230 and Alzheimer's Association Research Fellowship: AARF22973974 to A.F. and NIH/NIA grants R01AG069433 and AG073133 to G.T.

CONFLICT OF INTEREST STATEMENT

The authors declare no conflicts of interest. Author disclosures are available in the Supporting information.

CONSENT STATEMENT

Informed consent was obtained from all participants prior to their enrollment in the studies at the AD Center (ADC) at OHSU and at AD Center, Sanders-Brown Center on Aging at the University of Kentucky.

ORCID

Giulio Taglialatela https://orcid.org/0000-0003-4795-447X

REFERENCES

1. 2023 Alzheimer's disease facts and figures. Alzheimers Dement. *J Alzheimers Assoc*. 2023;19(4):1598-1695. doi:10.1002/alz.13016
2. Jellinger KA. Neuropathology of the Alzheimer's continuum: an update. *Free Neuropathol*. 2020;1:1-32. doi:10.17879/freeneuropathology-2020-3050
3. Chen G, Xu TH, Yan Y, et al. Amyloid beta: structure, biology and structure-based therapeutic development. *Acta Pharmacol Sin*. 2017;38(9):1205-1235. doi:10.1038/aps.2017.28
4. Braak H, Braak E. Neuropathological stageing of Alzheimer-related changes. *Acta Neuropathol (Berl)*. 1991;82(4):239-259. doi:10.1007/BF00308809
5. Igarashi KM. Entorhinal cortex dysfunction in Alzheimer's disease. *Trends Neurosci*. 2023;46(2):124-136. doi:10.1016/j.tins.2022.11.006
6. Rao YL, Ganaraja B, Murlimanju BV, Joy T, Krishnamurthy A, Agrawal A. Hippocampus and its involvement in Alzheimer's disease: a review. *3 Biotech*. 2022;12(2):55. doi:10.1007/s13205-022-03123-4
7. Spires-Jones TL, Hyman BT. The intersection of amyloid beta and tau at synapses in Alzheimer's disease. *Neuron*. 2014;82(4):756-771. doi:10.1016/j.neuron.2014.05.004
8. Lanz TA, Carter DB, Merchant KM. Dendritic spine loss in the hippocampus of young PDAPP and Tg2576 mice and its prevention by the ApoE2 genotype. *Neurobiol Dis*. 2003;13(3):246-253. doi:10.1016/S0969-9961(03)00079-2
9. Pozueta J, Lefort R, Shelanski ML. Synaptic changes in Alzheimer's disease and its models. *Neuroscience*. 2013;251:51-65. doi:10.1016/j.neuroscience.2012.05.050
10. Sehar U, Rawat Reddy AP, Kopel J, Reddy PH. Amyloid beta in aging and Alzheimer's disease. *Int J Mol Sci*. 2022;23(21):12924. doi:10.3390/ijms232112924
11. Zolochevska O, Taglialatela G. Non-demented individuals with Alzheimer's disease neuropathology: resistance to cognitive decline may reveal new treatment strategies. *Curr Pharm Des*. 2016;22(26):4063-4068.
12. Walker K, Herskowitz JH, Dendritic Spines: mediators of cognitive resilience in aging and Alzheimer's disease—courtney, 2021;27(5):487-505. Accessed: Nov. 08, 2023. [Online]. https://journals.sagepub.com/doi/full/10.1177/1073858420945964
13. Jack CR Jr, Bennett DA, Blennow K, et al. NIA-AA Research Framework: toward a biological definition of Alzheimer's disease. *Alzheimers Dement*. 2018;14(4):535-562. doi:10.1016/j.jalz.2018.02.018

14. Thal DR, Von Arnim C, Griffin WST, et al. Pathology of clinical and preclinical Alzheimer's disease. *Eur Arch Psychiatry Clin Neurosci*. 2013;263(2):137-145. doi:10.1007/s00406-013-0449-5
15. Xekardaki A, Kövari E, Gold G. Neuropathological changes in aging brain. in GeNeDis 2014. In: Vlamos P, Alexiou A, eds. *Advances in Experimental Medicine and Biology*. Springer International Publishing; 2015:11-17. doi:10.1007/978-3-319-08939-3_6
16. Boros BD, Greathouse KM, Gentry EG, et al. Dendritic spines provide cognitive resilience against Alzheimer's disease. *Ann Neurol*. 2017;82(4):602-614. doi:10.1002/ana.25049
17. Zolochevska O, Bjorklund N, Woltjer R, Wiktorowicz JE, Taglialatela G. Postsynaptic proteome of non-demented individuals with Alzheimer's disease neuropathology. *J Alzheimers Dis JAD*. 2018;65(2):659-682. doi:10.3233/JAD-180179
18. Briley D, Ghirardi V, Woltjer R, et al. Preserved neurogenesis in non-demented individuals with AD neuropathology. *Sci Rep*. 2016;6:27812. doi:10.1038/srep27812
19. Fracassi A, Marcatti M, Zolochevska O, et al. Oxidative damage and antioxidant response in frontal cortex of demented and non-demented individuals with Alzheimer's neuropathology. *J Neurosci Off J Soc Neurosci*. 2021;41(3):538-554. doi:10.1523/JNEUROSCI.0295-20.2020
20. Tumurbaatar B, Fracassi A, Scaduto P, et al. Preserved autophagy in cognitively intact non-demented individuals with Alzheimer's neuropathology. *Alzheimers Dement J Alzheimers Assoc*. 2023;19(12):5355-5370. doi:10.1002/alz.13074
21. Singh A, Allen D, Fracassi A, et al. Functional integrity of synapses in the central nervous system of cognitively intact individuals with high Alzheimer's disease neuropathology is associated with absence of synaptic tau oligomers. *J Alzheimers Dis JAD*. 2020;78(4):1661-1678. doi:10.3233/JAD-200716
22. Bjorklund NL, Reese LC, Sadagoparamanujam V-M, Ghirardi V, Woltjer RL, Taglialatela G. Absence of amyloid β oligomers at the postsynapse and regulated synaptic Zn2+ in cognitively intact aged individuals with Alzheimer's disease neuropathology. *Mol Neurodegener*. 2012;7:23. doi:10.1186/1750-1326-7-23
23. Algamal M, Russ AN, Miller MR, et al. Reduced excitatory neuron activity and interneuron-type-specific deficits in a mouse model of Alzheimer's disease. *Commun Biol*. 2022;5(1):1323. doi:10.1038/s42003-022-04268-x
24. Tsai J, Grutzendler J, Duff K, Gan W-B. Fibrillar amyloid deposition leads to local synaptic abnormalities and breakage of neuronal branches. *Nat Neurosci*. 2004;7(11):1181-1183. doi:10.1038/nn1335
25. Fracassi A, Marcatti M, Tumurbaatar B, Woltjer R, Moreno S, Taglialatela G. TREM2-induced activation of microglia contributes to synaptic integrity in cognitively intact aged individuals with Alzheimer's neuropathology. *Brain Pathol Zurich Switz*. 2023;33(1):e13108. doi:10.1111/bpa.13108
26. Yuste R. The discovery of dendritic spines by Cajal. *Front Neuroanat*. 2015;9:18. Accessed: Dec. 22, 2023. [Online]. https://www.frontiersin.org/articles/10.3389/fnana.2015.00018
27. Amaral MD, Pozzo-Miller L. The dynamics of excitatory synapse formation on dendritic spines. *Cellscience*. 2009;5(4):19-25.
28. Dorostkar MM, Zou C, Blazquez-Llorca L, Herms J. Analyzing dendritic spine pathology in Alzheimer's disease: problems and opportunities. *Acta Neuropathol (Berl)*. 2015;130(1):1-19. doi:10.1007/s00401-015-1449-5
29. Lacor PN, Buniel MC, Furlow PW, et al. Aβ oligomer-induced aberrations in synapse composition, shape, and density provide a molecular basis for loss of connectivity in Alzheimer's disease. *J Neurosci*. 2007;27(4):796-807. doi:10.1523/JNEUROSCI.3501-06.2007
30. Stallings NR, O'Neal MA, Hu J, Kavalali ET, Bezprozvanny I, Malter JS. Pin1 mediates Aβ42-induced dendritic spine loss. *Sci Signal*. 2018;11(522):eaap8734. doi:10.1126/scisignal.aap8734
31. Lu PJ, Wulf G, Zhou XZ, Davies P, Lu KP. The prolyl isomerase Pin1 restores the function of Alzheimer-associated phosphorylated tau protein. *Nature*. 1999;399(6738):784-788. doi:10.1038/21650
32. Antonelli R, De Filippo R, Midde S, et al. Pin1 modulates the synaptic content of NMDA receptors via prolyl-isomerization of PSD-95. *J Neurosci*. 2016;36(20):5437-5447. doi:10.1523/JNEUROSCI.3124-15.2016
33. Malter JS. Pin1 and Alzheimer's disease. *Transl Res J Lab Clin Med*. 2023;254:24-33. doi:10.1016/j.trsl.2022.09.003
34. Walker CK, Greathouse KM, Tuscher JJ, et al. Cross-platform synaptic network analysis of human entorhinal cortex identifies TWF2 as a modulator of dendritic spine length. *J Neurosci*. 2023;43(20):3764-3785. doi:10.1523/jneurosci.2102-22.2023
35. Swanger SA, Yao X, Gross C, Bassell GJ. Automated 4D analysis of dendritic spine morphology: applications to stimulus-induced spine remodeling and pharmacological rescue in a disease model. *Mol Brain*. 2011;4:38. doi:10.1186/1756-6606-4-38
36. Hampel H, Hardy J, Blennow K, et al. The amyloid-β pathway in Alzheimer's disease. *Mol Psychiatry*. 2021;26(10):5481-5503. doi:10.1038/s41380-021-01249-0
37. Lee A, Kondapalli C, Virga DM, et al. Aβ42 oligomers trigger synaptic loss through CAMKK2-AMPK-dependent effectors coordinating mitochondrial fission and mitophagy. *Nat Commun*. 2022;13(1):4444. doi:10.1038/s41467-022-32130-5
38. Pelucchi S, Gardoni F, Di Luca M, Marcello E. Synaptic dysfunction in early phases of Alzheimer's Disease. *Handb Clin Neurol*. 2022;184:417-438. doi:10.1016/B978-0-12-819410-2.00022-9
39. Holtmaat A, Wilbrecht L, Knott GW, Welker E, Svoboda K. Experience-dependent and cell-type-specific spine growth in the neocortex. *Nature*. 2006;441(7096):979-983. doi:10.1038/nature04783
40. Lin L, Lo LHY, Lyu Q, Lai KO. Determination of dendritic spine morphology by the striatin scaffold protein STRN4 through interaction with the phosphatase PP2A. *J Biol Chem*. 2017;292(23):9451-9464. doi:10.1074/jbc.M116.772442
41. Gipson CD, Olive MF. Structural and functional plasticity of dendritic spines—root or result of behavior? *Genes Brain Behav*. 2017;16(1):101-117. doi:10.1111/gbb.12324
42. Bączyńska E, Pels KK, Basu S, Włodarczyk J, Ruszczycki B. Quantification of dendritic spines remodeling under physiological stimuli and in pathological conditions. *Int J Mol Sci*. 2021;22(8):4053. doi:10.3390/ijms22084053
43. Pchitskaya E, Bezprozvanny I. Dendritic spines shape analysis – classification or clusterization? Perspective. *Front Synaptic Neurosci*. 2020;12:31. Accessed: Jan. 08, 2024. [Online]. https://www.frontiersin.org/articles/10.3389/fnsyn.2020.00031
44. Guo H, Ali T, Que J, Zhou Y, Bai Y. Dendritic spine dynamics in associative memory: a comprehensive review. *FASEB J*. 2023;37(5):e22896. doi:10.1096/fj.202202166R
45. Mao YT, Zhu JX, Hanamura K, Iurilli G, Datta SR, Dalva MB. Filopodia conduct target selection in cortical neurons using differences in signal kinetics of a single kinase. *Neuron*. 2018;98(4):767-782.e8. doi:10.1016/j.neuron.2018.04.011
46. Hering H, Sheng M. Dentritic spines: structure, dynamics and regulation. *Nat Rev Neurosci*. 2001;2(12):880-888. doi:10.1038/35104061
47. Bello-Medina PC, Flores G, Quirarte GL, McGaugh JL, Prado Alcalá RA. Mushroom spine dynamics in medium spiny neurons of dorsal striatum associated with memory of moderate and intense training. *Proc Natl Acad Sci*. 2016;113(42):E6516-E6525. doi:10.1073/pnas.1613680113
48. Xu L, Ren Z, Chow FE, et al. Pathological role of peptidyl-prolyl isomerase pin1 in the disruption of synaptic plasticity in Alzheimer's disease. *Neural Plast*. 2017;2017:3270725. doi:10.1155/2017/3270725
49. Mevel K, Chételat G, Eustache F, Desgranges B. The default mode network in healthy aging and Alzheimer's disease. *Int J Alzheimers Dis*. 2011;2011:535816. doi:10.4061/2011/535816

50. Lauterborn JC, Scaduto P, Cox CD, et al. Increased excitatory to inhibitory synaptic ratio in parietal cortex samples from individuals with Alzheimer's disease. *Nat Commun*. 2021;12(1):2603. doi:10.1038/s41467-021-22742-8
51. Mijalkov M, Volpe G, Fernaud-Espinosa I, DeFelipe J, Pereira JB, Merino-Serrais P. Dendritic spines are lost in clusters in Alzheimer's disease. *Sci Rep*. 2021;11(1):12350. doi:10.1038/s41598-021-91726-x
52. Kurucu H, Colom-Cadena M, Davies C, et al. Inhibitory synapse loss and accumulation of amyloid beta in inhibitory presynaptic terminals in Alzheimer's disease. *Eur J Neurol*. 2022;29(5):1311-1323. doi:10.1111/ene.15043
53. Griffiths J, Grant SGN. Synapse pathology in Alzheimer's disease. *Semin Cell Dev Biol*. 2023;139:13-23. doi:10.1016/j.semcdb.2022.05.028
54. Subramanian J, Savage JC, Tremblay MÈ. Synaptic loss in Alzheimer's disease: mechanistic insights provided by two-photon in vivo imaging of transgenic mouse models. *Front Cell Neurosci*. 2020;14:592607. doi:10.3389/fncel.2020.592607
55. Koffie RM, Meyer-Luehmann M, Hashimoto T, et al. Oligomeric amyloid β associates with postsynaptic densities and correlates with excitatory synapse loss near senile plaques. 2009;106(10):4012-4017. doi:10.1073/pnas.0811698106
56. Célestine M, Jacquier-Sarlin M, Borel E, et al. Long term worsening of amyloid pathology, cerebral function, and cognition after a single inoculation of beta-amyloid seeds with Osaka mutation. *Acta Neuropathol Commun*. 2023;11(1):66. doi:10.1186/s40478-023-01559-0
57. Runge K, Cardoso C, de Chevigny A. Dendritic spine plasticity: function and mechanisms. *Front Synaptic Neurosci*. 2020;12. Accessed: Jan. 08, 2024. [Online]. https://www.frontiersin.org/articles/10.3389/fnsyn.2020.00036
58. Kommaddi RP, Das D, Karunakaran S, et al. Aβ mediates F-actin disassembly in dendritic spines leading to cognitive deficits in Alzheimer's disease. *J Neurosci Off J Soc Neurosci*. 2018;38(5):1085-1099. doi:10.1523/JNEUROSCI.2127-17.2017
59. Chung WS, Allen NJ, Eroglu C. Astrocytes control synapse formation, function, and elimination. *Cold Spring Harb Perspect Biol*. 2015;7(9):a020370. doi:10.1101/cshperspect.a020370
60. Haber M, Zhou L, Murai KK. Cooperative astrocyte and dendritic spine dynamics at hippocampal excitatory synapses. *J Neurosci Off J Soc Neurosci*. 2006;26(35):8881-8891. doi:10.1523/JNEUROSCI.1302-06.2006
61. Schikorski T, Stevens CF. Quantitative ultrastructural analysis of hippocampal excitatory synapses. *J Neurosci Off J Soc Neurosci*. 1997;17(15):5858-5867. doi:10.1523/JNEUROSCI.17-15-05858.1997
62. Holderith N, Lorincz A, Katona G, et al. Release probability of hippocampal glutamatergic terminals scales with the size of the active zone. *Nat Neurosci*. 2012;15(7):988-997. doi:10.1038/nn.3137
63. Targa Dias Anastacio H, Matosin N, Ooi L. Neuronal hyperexcitability in Alzheimer's disease: what are the drivers behind this aberrant phenotype? *Transl Psychiatry*. 2022;12(1):257. doi:10.1038/s41398-022-02024-7
64. Gail Canter R, Huang WC, Choi H, et al. 3D mapping reveals network-specific amyloid progression and subcortical susceptibility in mice. *Commun Biol*. 2019;2:360. doi:10.1038/s42003-019-0599-8
65. Westmark PR, Westmark CJ, Wang S, et al. Pin1 and PKMζ sequentially control dendritic protein synthesis. *Sci Signal*. 2010;3(112):ra18-ra18. doi:10.1126/scisignal.2000451
66. Kimura T, Tsutsumi K, Taoka M, et al. Isomerase Pin1 stimulates dephosphorylation of tau protein at cyclin-dependent kinase (Cdk5)-dependent Alzheimer phosphorylation sites. *J Biol Chem*. 2013;288(11):7968-7977. doi:10.1074/jbc.M112.433326
67. Wang L, Zhou Y, Chen D, Lee TH. Peptidyl-prolyl cis/trans isomerase Pin1 and Alzheimer's disease. *Front Cell Dev Biol*. 2020;8. Accessed: Jan. 03, 2024. [Online]. https://www.frontiersin.org/articles/10.3389/fcell.2020.00355
68. Silva JD, Taglialatela G, Jupiter DC. Reduced prevalence of dementia in patients prescribed tacrolimus, sirolimus, or cyclosporine. *J Alzheimers Dis JAD*. 2023;95(2):585-597. doi:10.3233/JAD-230526
69. Taglialatela G, Rastellini C, Cicalese L. Reduced incidence of dementia in solid organ transplant patients treated with calcineurin inhibitors. *J Alzheimers Dis JAD*. 2015;47(2):329-333. doi:10.3233/JAD-150065
70. Pastorino L, Sun A, Lu PJ, et al. The prolyl isomerase Pin1 regulates amyloid precursor protein processing and amyloid-beta production. *Nature*. 2006;440(7083):528-534. doi:10.1038/nature04543

SUPPORTING INFORMATION

Additional supporting information can be found online in the Supporting Information section at the end of this article.

How to cite this article: Guptarak J, Scaduto P, Tumurbaatar B, et al. Cognitive integrity in Non-Demented Individuals with Alzheimer's Neuropathology is associated with preservation and remodeling of dendritic spines. *Alzheimer's Dement*. 2024;20:4677–4691. https://doi.org/10.1002/alz.13900